Journal of Non-Crystalline Solids 414 (2015) 7–15

Contents lists available at ScienceDirect

Journal of Non-Crystalline Solids

journal homepage: www.elsevier.com/ locate/ jnoncrysol

Short- and medium-range orders in as-quenched and deformed SiO_2 glasses: An atomistic study

P. Koziatek [a,b], J.L. Barrat [b], D. Rodney [a,c,*]

[a] Science et Ingénierie des Matériaux et Procédés, Grenoble INP, CNRS/UJF, 38402 Saint Martin d'Hères, France
[b] Laboratoire Interdisciplinaire de Physique, Université Joseph Fourier Grenoble, CNRS, 38402 Saint Martin d'Hères, France
[c] Institut Lumière Matière, Université Claude Bernard Lyon 1, CNRS, 69622 Villeurbanne, France

ARTICLE INFO

Article history:
Received 16 September 2014
Received in revised form 6 January 2015
Accepted 13 January 2015
Available online xxxx

Keywords:
Silica;
Simulation;
Pressure;
Polyamorphism;
Potential energy landscape

ABSTRACT

Using a truncated BKS interatomic potential, we compare the coordination number, ring size distribution and distributions of activation energies in silica glasses of different densities processed with two different routes: either directly quenched from the high temperature melt at different densities, or deformed from an ambient temperature, low density glass through cycles of quasistatic compression–decompression. We find that the coordination number and ring size distribution vary simultaneously in both quenched and deformed glasses and are irreversible in compressed glasses unloaded to zero pressure, but are surprisingly close to reversible (with a hysteresis) when the decompressions are continued back to the initial density. At a given density, the pressure is significantly lower in quenched glasses than in compressed glasses but the coordination number and ring size distribution are unexpectedly similar, showing that their evolution during compression is mostly a steric effect. Also, distributions of activation energies in quenched and deformed glasses are significantly different, with the deformed glasses showing the classical overabundance of low activation energies characteristic of far-from-equilibrium systems.

1. Introduction

Silica is ubiquitous in nature and technology, being a base constituent of the earth mantle as well as of most commercial glasses [1]. Silica also exhibits a very unique and fascinating behavior under pressure, which is not fully understood.

There is a general consensus that experimentally, silica glasses are elastic up to about 10 GPa but show a surprising non-monotonous variation of the bulk modulus with a minimum at around 2–3 GPa [2–5]. Above 10 GPa, silica glasses enter a plastic regime marked by permanent densification upon decompression [2,3,5]. The densification increases gradually with the maximum applied pressure and saturates at about 20% above 25 GPa [6]. Based mainly on Raman spectroscopy measurements [7,8], densification was shown to occur through an alteration of the medium range order (MRO) in the glass. Silica has a three-dimensional network structure forming paths of successive Si–O–Si bonds organized inside corner-sharing tetrahedra. The MRO has been characterized by the size distribution of closed paths, or rings [9,10] and densification was shown to be related to an increase in the population of small three- and four-membered rings [11,12]. In analogy with crystalline polymorphism [3], this pressure-induced transition has been described as an evidence of polyamorphism, with the permanent densification observed after decompression corresponding to a progressive transformation from a low-density amorphous (LDA) structure to a high-density amorphous (HDA) structure. Both decompressed structures have the same SRO (tetrahedral structures) but different MROs. We should note however that the mechanism relating densification to a change of MRO is not clear to this date.

Also, X-ray diffraction measurements evidenced a structural transition, which affects the short-range order (SRO) in the glass, i.e. the Si coordination number, as shown in the pioneering work of Meade et al. [13]. Through the transition, the number of first-neighbor oxygen atoms of the Si atoms increases from 4 to 6, such that the tetrahedral structure observed at ambient pressure is transformed into an octahedral structure at high pressure [14]. In contrast with the MRO transition which is irreversible upon decompression, this second transition was found experimentally to be reversible. After decompression, the densified glass contains only fourfold coordinated Si atoms [15]. The pressure range over which this transition occurs and its potential overlap with the MRO transition are matters of heated debates [16–18,6,19], arising partly because different ranges of pressures for the SRO transition have been reported experimentally. Early X-ray diffraction measurements showed a constant coordination number up to at least 8 GPa [13], but more recently, transitions were reported from 15 GPa [14] or above, 20 GPa [20,18], which implies that the SRO transition occurs at higher pressure than the MRO transition. However, using X-ray Raman scattering [15], the SRO transition was found to start at around

* Corresponding author at: Institut Lumière Matière, Université Claude Bernard Lyon 1, CNRS, 69622 Villeurbanne, France.
E-mail address: david.rodney@univ-lyon1.fr (D. Rodney).

http://dx.doi.org/10.1016/j.jnoncrysol.2015.01.009
0022-3093/

10 GPa and end at around 25 GPa, thus fully overlapping with the MRO transition. Interestingly, most published works focus either on the SRO or the MRO transition. These transitions are studied using different techniques that provide different information, vibrational modes for Raman spectroscopy and structure factor for X-ray diffraction. Since depending on the reports, the pressure ranges of the transitions may or may not overlap, we cannot say whether both transitions are the two faces of a single structural transformation or are distinct transitions.

On the modeling side, atomistic simulations have proved essential in the study of amorphous systems, despite their strong limitations in both time- and length-scales [21]. Concerning silica, simulations reproduce a minimum in the bulk modulus [22–24] although the pressure at the minimum is usually larger than in experiments and close (or equal) to the elastic limit, which itself is lower than experimentally, 6–8 GPa [25–27,24]. Densification after decompression from the plastic regime is also reproduced but the latter is almost systematically attributed in the modeling studies to an increase in the Si coordination number, i.e. the SRO transition. The reason is that in atomistic simulations, the onset of the plastic regime is systematically marked by the appearance of fivefold coordinated Si atoms [25–28,23,29,24,19]. Interestingly, in the modeling community and in contrast with the experimental interpretation, densification is thus related to the SRO and not the MRO transition. One exception is the work of Huang and Kieffer [30,22] who used an interatomic potential which did not allow the coordination number to vary and still observed a densification once the glass enters the plastic regime. In this case, densification is thus related to a change in the ring size distribution, but we should note that the simulations showed the appearance of large rings, while experimentally, it is the fraction of small rings that increases [7]. Moreover, as in experiments, numerical works tend to focus either on the SRO or the MRO and a detailed study of both transitions treated on equal footing is still missing.

To progress in this debate, we take here a computational point-of-view and use an atomistic model of silica glasses, on which we measure simultaneously the MRO (ring size distribution) and SRO (coordination number). Moreover, we compare two radically different routes to vary the pressure and density of the glasses. The first route consists in applying quasistatic cycles of compression–decompression, as done in the past [24]. The second route is by quenching glasses directly from the high temperature melt at different densities and quench rates. Although there is no causal link between the different quenched configurations, this second route may be considered as corresponding to a very slow deformation where the glass is significantly annealed and relaxes partially between deformation increments. We also characterize the structure of the as-quenched and deformed glasses by exploring their potential energy landscape to determine the distribution of elementary thermally-activated events in these glasses. Our aim here is to determine whether the SRO and MRO transitions are distinct within our numerical model and to study in details how the history of the glass (quenched or deformed, quench rate, density) affects its structure and properties.

2. Methodology

We represent atomic bonding in silica with the two-body potential developed by van Beest, Kramer and van Santen (BKS) [31] and modified by Carré et al. [32] to replace the long-range Coulombic interaction by a Wolf truncation. The parameters of the potential are given in Ref. [24]. The BKS potential has been used many times in the past and is known to reproduce the main structural and mechanical properties of silica, see for instance Refs. [33,34,32,29,24]. In particular under pressure, the BKS potential is known to reproduce the elastic limit, i.e. the pressure required to induce plasticity in the glass, as well as the pressure–densification curve [24].

The glasses considered here contain 3,000 atoms (1,000 Si atoms, 2,000 O atoms) in cubic periodic simulation cells. They were obtained from a melt equilibrated at 5200 K and quenched at constant volume down to 0 K at different quench rates varying between 5.2 10^{14} K/s down to 5.2 10^{11} K/s, thus covering 4 orders of magnitude. Glasses were prepared in cells of different volumes to vary their density between 2.2 and 3.4 g/cm^3.

A reference glass, quenched at 5.2 10^{11} K/s with a density of 2.2 g/cm^3, was then used to simulate cycles of hydrostatic compression–decompression. The cycles were density-controlled, returning to the initial density after compressions up to varying pressures. The deformations were applied quasistatically by changing the volume by small increments ($\delta V/V = 10^{-4}$) followed by energy minimizations with a force tolerance of 10^{-3} eV/Å. We also performed molecular dynamics deformations at constant strain rate ($\delta \dot{V}/V = 10^{9}$ s^{-1}) and constant temperature (1200 K), but the results were the same as for the quasistatic deformations and will not be presented here.

To analyze the short- and medium-range orders, we identify the first neighbors of the Si atoms from a Voronoi tessellation, as in the work of Sheng et al. [35]. The tessellations are obtained with the Voro++ software [36] and give access to the coordination number of the Si atoms and the fractions of 4-, 5- and 6-fold coordinated atoms. To determine the ring statistics, we employed a shortest path analysis [37,30,38] where the smallest ring that connects every pair of Si–O bonds on every Si atom is determined. The rings have sizes between 3 and 7 (i.e. they contain from 6 to 14 consecutive Si–O bonds). Two-membered rings, which correspond to two edge-sharing tetrahedra, are very rare and were omitted here, as well as very large rings with sizes above 7.

Finally, the potential energy landscape of the as-quenched and deformed glasses is explored using the activation–relaxation technique (ART) [39], as implemented in Refs. [40,41] and often applied in the past to fragile glasses modeled with Lennard-Jones (LJ) potentials [42,21,43,44]. ART is eigenvector-following method, which requires only the knowledge of an initial equilibrium configuration. Saddle-points are searched along random directions in the neighborhood of the initial configuration by first choosing a random direction in configuration space, second, moving the system along this direction until the configuration becomes unstable, i.e. the Hessian matrix acquires a negative eigenvalue, and third, following the corresponding eigenvector, which will lead to a saddle-point of first order. The reader interested in more technical details is referred to Ref. [41]. Random searches were iterated until at least 1,000 distinct saddles were found for each configuration. Eigenfrequencies were then determined by diagonalizing the Hessian matrix of the initial configuration and of each activated state [45]. The searches start in a direction of configuration space, which corresponds to the random motion of atoms inside a sphere of specified radius centered on a random atom. If the sphere radius is small (less than the first neighbor distance), a single atom initially moves but in practice, all attempts systematically failed when an Si atom was picked. Only attempts starting with an O atom succeeded. In order to stimulate Si atoms, a larger sphere radius had to be used (4 Å), involving then the initial displacement of about 10 atoms and leading to transitions that involved Si atoms with their surrounding O first-neighbors.

3. As-quenched glasses

We start by considering the structure and properties of undeformed glasses quenched at different quench rates and densities.

3.1. Pressure and energy

Fig. 1 shows the pressure and average potential energy per atom of as-quenched glasses as a function of their density. As expected, we see in Fig. 1(b) that glasses quenched more slowly have a lower energy, i.e. they are better relaxed. Moreover, for each quench rate there is a density, which minimizes the glass energy. Although the data is somewhat noisy, we can see that the minimum-energy density tends to shift

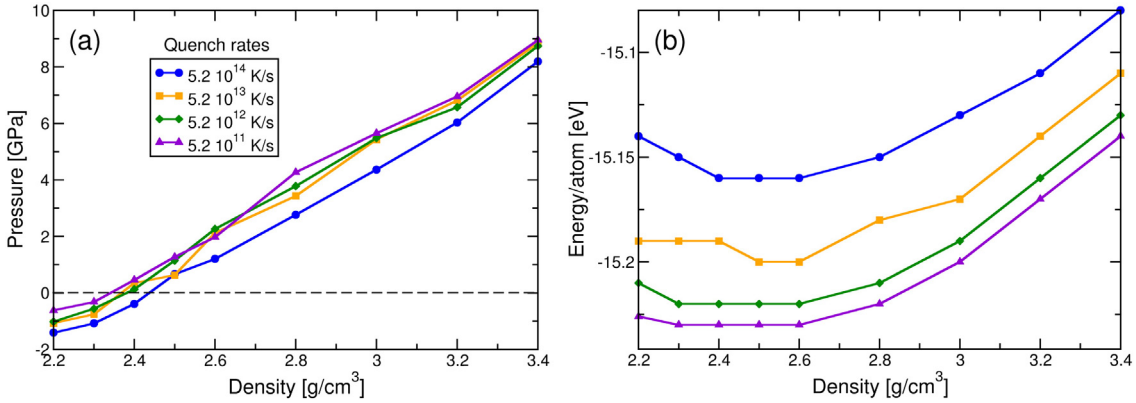

Fig. 1. Pressure (a) and average energy per atom (b) as a function of density for glasses quenched at different quench rates given in (a).

towards lower densities when the glass is quenched more slowly; that is, better relaxed glasses are less dense. This is confirmed by the pressure curves in Fig. 1(a), which shift towards lower densities when the quench rate is decreased. In particular, the equilibrium density at which the pressure P is zero, which corresponds to the minimum-energy density in Fig. 1(b) since $P = -dE/dV$, varies from about 2.45 down to 2.35 g/cm^3 when the quench rate is decreased by 4 orders of magnitude. As discussed in Ref. [33], the decrease in density is related to an opening of the SiO_4 tetrahedral structure in better relaxed glasses, where the tetrahedra become more regular and rotate away from each other as evidenced by an increase in the $\theta_{Si-O-Si}$ angle between adjacent tetrahedra.

3.2. Short range order

Fig. 2 shows the distributions of 4-, 5- and 6-fold coordinated Si atoms in the as-quenched glasses as a function of density, for the slowest and fastest quench rates. The best relaxed glasses contain only 4-fold coordinated Si atoms at low densities and are thus composed of a perfect network of interconnected tetrahedra, with no coordination defect. The least relaxed glasses on the other hand contain a few percents of 5-fold coordinated atoms even at low densities. At higher densities, the best relaxed glasses retain their perfect tetrahedral structure up to about 2.6 g/cm^3, which corresponds to a pressure of about 2 GPa (see Fig. 1(a)), while the least relaxed glasses see their fraction of 5-fold coordinated atoms increase already at low densities. For both glasses however, the trend is similar: the 5-fold coordinated atoms appear first, followed by 6-fold coordinated atoms at higher densities, around 2.9 g/cm^3. Consequently, as shown in the inset of Fig. 2, the average coordination number in the best relaxed glasses remains equal to 4 up to 2.6 g/cm^3 and then increases up to 4.6 at high pressures. The coordination number of the least relaxed glasses increases already at low densities but tends to the same asymptote as the relaxed glasses at high densities.

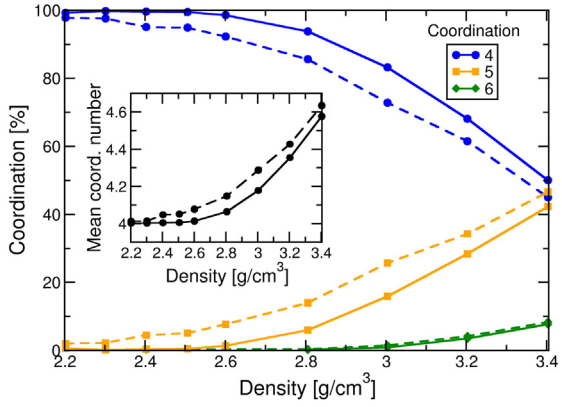

Fig. 2. Short-range order in as-quenched glasses: Fractions of 4-, 5- and 6-fold coordinated Si atoms in as-quenched glasses as a function of density. The solid (resp. dashed) line corresponds to the most slowly (resp. rapidly) quenched glass. The inset shows the resulting average coordination number as a function of density.

The tetrahedral structure is therefore more stable in the best relaxed glasses. As will be seen in the following, the trends shown here are typical of compressed glasses when they enter the plastic regime, the plastic events damaging the tetrahedral structure and creating coordination defects, initially 5-fold, then 6-fold. The creation of the defective atoms is therefore not a property of the plastic events but may arise solely from the topological constraints associated with high densities and steric effects.

3.3. Medium range order

Fig. 3 shows the statistics of the ring size distribution as a function of the cooling rate on the left and as a function of density on the right, for the best relaxed glasses. For all cooling rates, 6-membered rings are the most abundant at low density, which is expected for regular networks in analogy with the cristobalite structure, the low-pressure crystalline phase of silica, which is composed of only 6-membered rings. Moreover, we see from Fig. 3(a) that the ring size distribution is not strongly dependent on the quench rate. As a function of density (Fig. 3(b)), small and intermediate rings (3-, 4- and 5-membered rings) increase in proportion with increasing density, while larger rings (6- and 7-membered rings) decrease, such that above 2.8 g/cm^3, the most abundant rings have a size of 5. The stability of the rings as a function of density slightly depends on their size: 6-membered rings start to disappear at low densities (around 2.3 g/cm^3) while the other rings are more stable and start to vary only at around 2.6 g/cm^3, particularly the 3-membered rings, which appear only above about 2.8 g/cm^3.

From this first study of quenched glasses, we conclude that with the exception of 6-membered rings, the ring distribution in the quenched glasses starts to vary due to steric effects at the same density, about 2.6 g/cm^3, as the coordination number, which corresponds to a rather low pressure of about 2 GPa. Changes in SRO and MRO, which reflect a degradation of the tetrahedral structure, are thus concomitant, which can be understood intuitively since increasing the connectivity of the Si atoms necessarily implies shorter paths.

4. Deformed glasses

We now consider glasses quasistatically compressed up to 30 GPa.

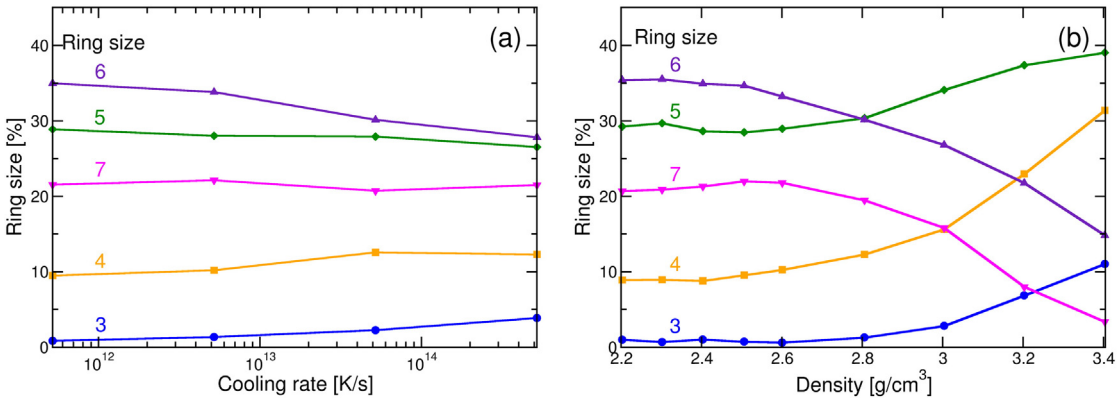

Fig. 3. Medium range order in as-quenched glasses: Ring size distributions as a function of (a) cooling rate (density 2.2 g/cm^3) and (b) density for the most slowly quenched glasses.

4.1. Mechanical curve

Fig. 4 shows the evolution of the pressure in the deformed glass as a function of density and a comparison on the left with as-quenched glasses and experimental data. The quasistatic pressure curve is similar to that obtained by Mantisi et al. [24]. The plastic regime is marked by large pressure drops, which correspond to the elastic pressure released by plastic events, although small plastic events (microplasticity [24]) occur almost right from the beginning of the compression, at about 2 GPa. Plasticity is accompanied with permanent densification upon decompression down to zero pressure. Decompressions up to at least 5 GPa are fully reversible and not shown here, while as seen in Fig. 4(a), a decompression from 8 GPa down yields a small densification at 0 GPa. The latter increases with the maximum pressure of the compression–decompression cycle, up to about 25 GPa, beyond which the densification saturates, as seen in the inset of Fig. 4(a). Densification is also marked by a decrease in the intertetrahedral angle, $\theta_{Si-O-Si}$.

This densification is well-known experimentally [46,3,8,5] and reproduced by several interatomic potentials [26,22,23,29,24]. Note that when the decompressions are continued until the initial density is recovered, the glass gets in tension with a final tensile pressure, which also increases with the maximum cycle pressure and saturates beyond about 25 GPa.

Fig. 4(b) shows that the quasistatic pressure is close to the experimental data, at least up to about 10 GPa beyond which the pressure in the experiments goes over the simulations. We note also that the curvature of the simulated pressure, which is related to the derivative of the bulk modulus with respect to density, does not change sign until the plastic regime. Hence, within the present model, the minimum of the effective bulk modulus corresponds to the elastic limit [24]. Also, the quasistatic pressure is much larger than the pressure in the as-quenched glasses. If the glasses after deformation were annealed long enough, we may expect the pressure to relax down to that of the as-quenched glasses, but quasistatic deformation, which does not allow for thermally-activated events, prevents such relaxations. The fact that the quasistatic pressure is close to the experimental pressure means that in experimental conditions, thermal activation does not play an important role either, or said in other words, the α-relaxation time, which sets the characteristic time for structural relaxations, is much longer than the characteristic time of the deformation, which is related to the inverse of the strain rate.

4.2. Short range order

Fig. 5 shows the fraction of 4-, 5- and 6-fold coordinated atoms and the corresponding average coordination number as a function of pressure and density, with comparisons with as-quenched glasses. As in as-quenched glasses, the fraction of 4-fold coordinated atoms starts to decrease when 5-fold coordinated atoms appear, followed at higher pressure by 6-fold coordinated atoms. As a result, the average coordination number in Fig. 5(e) starts to increase at about 5 GPa. However, as shown in the inset of Fig. 5(f), this variation is reversible upon decompression to zero pressure up to a maximum cycle pressure of

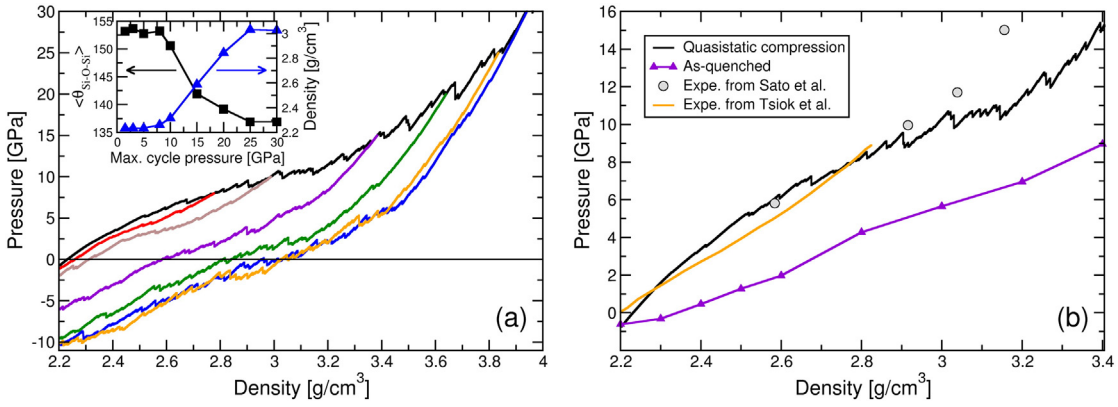

Fig. 4. Mechanical curve: (a) Pressure–density curve for the quasistatically deformed glass, with the compression in black and decompressions from different maximum pressures in various colors, (b) comparison between the pressure–density curves obtained on the one hand numerically by quasistatic compression (black) and by quench with the slowest numerical quench rate (denoted "as-quenched", purple) and on the other hand, obtained experimentally by Tsiok et al. [4] (orange curve) and Sato and Funamori [16] (circles). The inset in (a) shows the average intertetrahedral angle and density, both after decompressions to zero pressure, as a function of the maximum pressure reached in the cycle. (For interpretation of the references to color in this figure legend, the reader is referred to the web version of this article.)

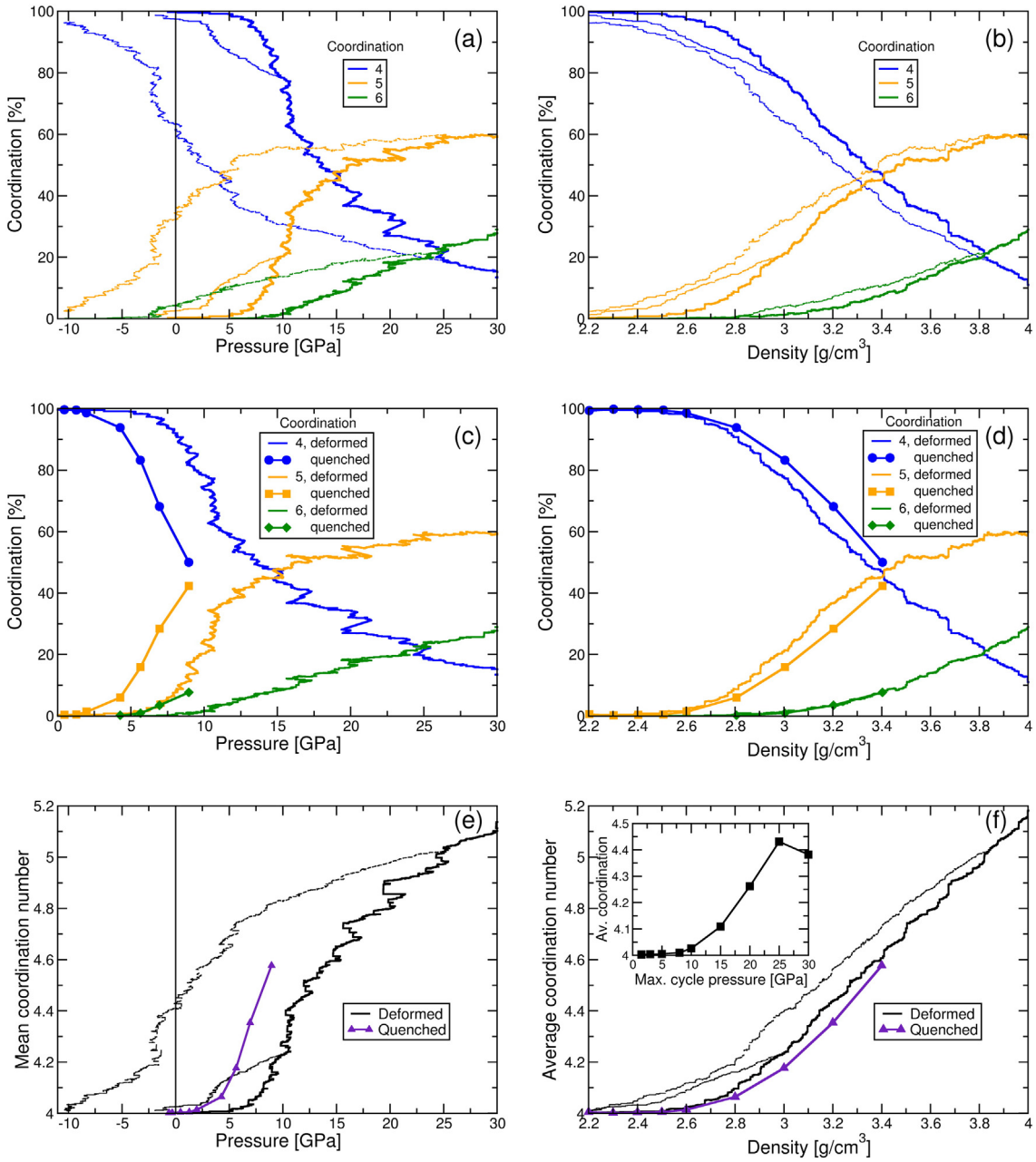

Fig. 5. Short range order in deformed glasses: fractions of 4-, 5- and 6-fold coordinated Si atoms as a function of (a) pressure and (b) density, (c–d) comparison with as-quenched glasses, (e–f) average coordination number. Decompressions from 10 and 25 GPa are shown as dashes lines in (a–b) and (e–f). Deformed glasses are shown as lines, as-quenched glasses as connected symbols as indicated in the legends. The inset in (f) shows the average coordination number in glasses decompressed to zero pressure as a function of the maximum pressure reached in the deformation cycle.

about 8 GPa. The evolution of the SRO thus becomes irreversible at the same pressure as the densification.

Beyond 8 GPa, the coordination number becomes strongly irreversible when unloaded to 0 GPa. For a decompression from 25 GPa, the fraction of 4-fold coordinated atoms is only about 60%, due to a large fraction of 5-fold coordinated atoms, close to 35%, while the 6-fold coordinated atoms remain in small proportion (less than 5%). This is in contrast with experiments, where the SRO transition is reported to be reversible [15]. On the other hand, it is very interesting to note that as a function of density, the coordination number shows a hysteresis but is close to fully reversible when the glass is brought back to its initial density. As seen in Fig. 5(e), the average coordination number, which is 4.4 at 0 GPa, is back to 4 at the end of the unloading, when the density is back to 2.2 g/cm^3. At this density, no 6-fold coordinated atoms remain, 5-fold coordinated atoms are only a few percents and about 98% of the atoms are back to being 4-fold coordinated.

The coordination number changes in as-quenched glasses take place at lower pressures than in deformed glasses, but the curves in Fig. 5(b), (d) and (f) are all close to superimposed when plotted as a function of density. The reason is that the pressure in the as-quenched glasses is significantly lower than in the quasistatically deformed glass Fig. 4(b). This means that during a compression, the SRO of the glass is mainly a function of the density and we may produce glasses with the same density and SRO but largely different pressures. The same is true for glasses brought back to their initial density, but not for any other density upon decompression because there is a hysteresis. With the exception of glasses recovered to their initial density, decompressed glasses at a given density have different SROs and MROs than as-quenched or

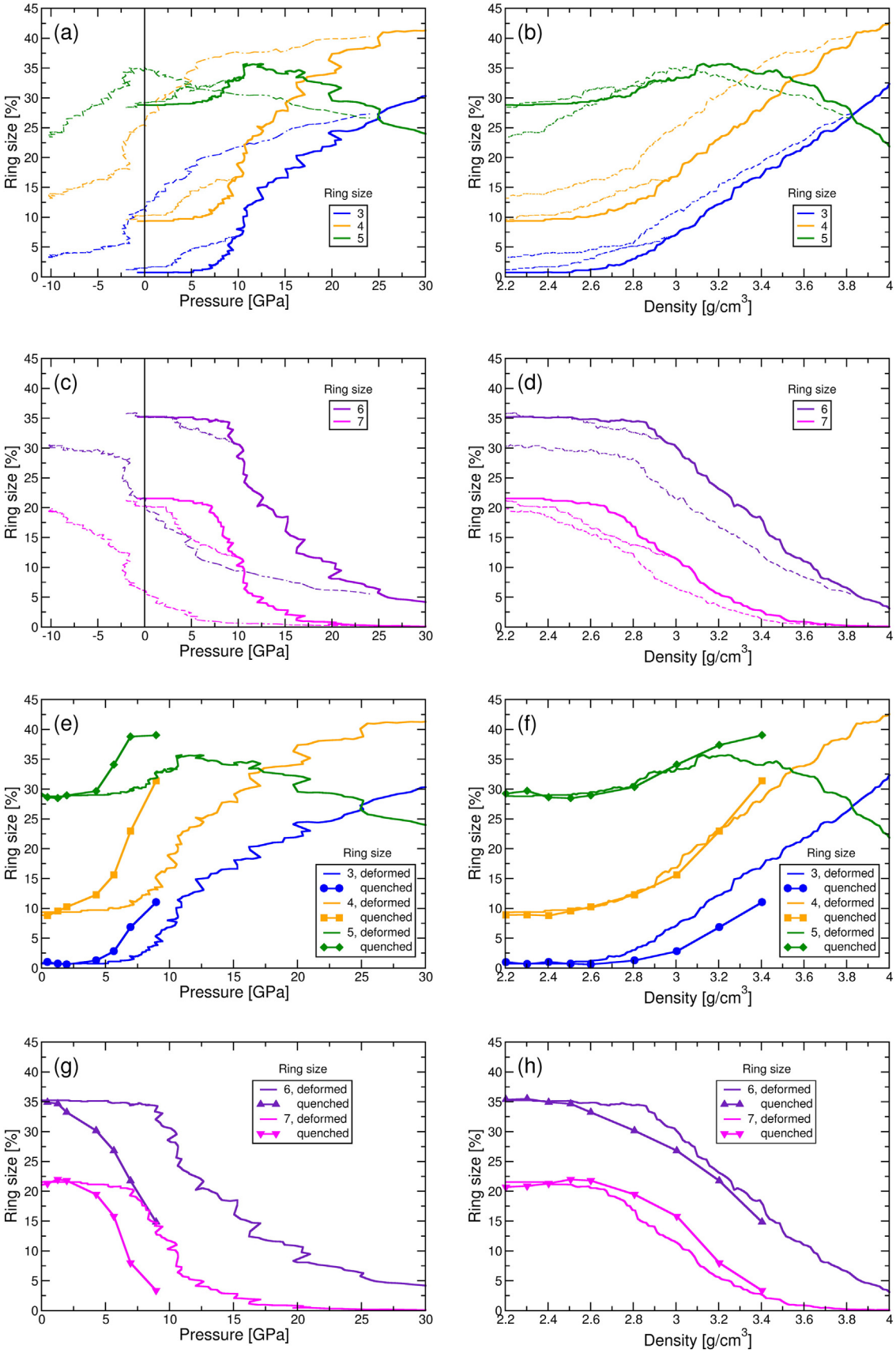

Fig. 6. Medium range order in deformed glasses: fractions of 3-, 4-, 5-membered rings as a function of (a) pressure and (b) density, (c–d) similar curves for 6- and 7-membered rings, (e–h) comparison with as-quenched glasses. Decompressions from 10 and 25 GPa are shown as dashed lines. Deformed glasses are shown as lines, as-quenched glasses as connected symbols as indicated in the legends. Small and intermediate rings (sizes 3 to 5) are separated from the larger rings (sizes 6 and 7) for the sake of clarity.

compressed glasses. The same behavior and conclusion can be made about the medium range order, as we will see below.

4.3. Medium range order

Fig. 6 shows the evolution of the ring size statistics as a function of pressure and density. Small rings (3- and 4-membered) increase in proportion during deformation, large rings (6- and 7-membered) decrease, while intermediate rings (5-membered) tend to remain relatively stable. Small and intermediate rings start to increase at around 5 GPa, while larger rings start to decrease at a slightly larger pressure and density. The same remarks made for the coordination apply here: irreversible changes in the ring size distribution start only after decompression from pressures at least 8 GPa as shown in Fig. 7, the changes are then strongly irreversible upon decompression to 0 GPa, with a marked increase in small rings and a marked decrease in large rings, but on the other hand, after decompression down to the initial density, the glass is back to a structure close to its initial structure. Differences are larger for the MRO than the SRO but remain on the order of 5%, which is small compared to the differences between the original and zero-pressure recovered glasses. Also, comparing as-quenched and deformed glasses, we see that in terms of pressure, the ring structure evolves at lower pressures in the as-quenched glasses, but as a function of density, both types of glasses have very similar evolutions, with maybe the exception of 3-membered rings, which increase in proportion more slowly in as-quenched glasses than in deformed glasses Fig. 6(f).

4.4. Potential energy landscape

In this section, we discuss the potential energy landscape of the silica glasses as determined by the activation–relaxation technique (ART). As mentioned in Section 2, depending on the initial search direction in configuration space, the thermally-activated paths identified here involve either only the motion of O atoms, or the motion of Si atoms along with some of their O first neighbors. Fig. 8(a) and (b) shows the corresponding distributions of activation energies. Based on our transition path sampling, when only O atoms are involved (Fig. 8(a)), the transitions mainly involve the exchange of O atoms between Si atoms, the lowest barriers corresponding to the exchange of just 2 O atoms, while higher energy barriers may involve up to 5–6 O atoms, shuffling between Si atoms. Most of these events have very high activation energies, 6 to 8 eV, because they require breaking strong attractive bonds between Si and O atoms.

When both Si and O atoms are involved (Fig. 8(b)), the activation energies are shifted towards lower activation energies. The lowest activation energies correspond to a partial rotation of a silicon with its nearest O neighbors, i.e. the elementary event involved in the α- to β-cristobalite transition, which is often mentioned at the origin of the non-monotonous variation of the bulk modulus in the elastic regime [30,23] and is similar to the double well potential processes reported in Ref. [34]. For higher energy barriers, the transitions involve larger displacements of Si atoms, dragging along the O atoms from their neighborhood. From our transition path sampling, we observed that the number of O atoms involved in a transition never exceeded 9. During these events, both the coordination number and ring size vary.

Fig. 8(a) and (b) also shows the activation energy distributions for four different quench rates, where a well-known trend is observed [21,44]: glasses quenched more slowly have fewer low activation energy transitions, i.e. they are surrounded by higher activation barriers.

Fig. 8(c) shows the activation energy distributions in glasses quenched at the same quench rate ($5.2\ 10^{11}$ K/s) but with different densities. We see a shift of the activation energies towards lower energies when the density increases. This is to be related to the alteration of the perfect tetrahedral structure at high densities reported in Section 3. Similarly, we see in Fig. 8(d) that glasses after deformation contain a high density of low activation energies. This effect is well-known in LJ glasses [21,44]: the plastic deformation takes the glass away from its initial low energy state and brings it to a high energy state, which is less stable and therefore surrounded by lower activation barriers. However, we should note that the appearance of low activation energies is progressive as a function of the maximum pressure reached in the cycle.

It was recently reported in the case of LJ glasses [44] that the attempt frequencies, which are usually thought of as constant, are in fact extremely widely spread among activated events, varying by almost 10 orders of magnitude between the smallest and largest frequencies. Within the harmonic transition state theory, the attempt frequency is expressed as the ratio of the product of the eigenfrequencies of the system computed in the activated and initial configurations. As mentioned in Section 2, the eigenfrequencies are obtained by diagonalizing the Hessian matrix of the system. The resulting attempt frequencies are shown in Fig. 9 for two silica glasses quenched at different quench rates and for a glass before and after a cycle of compression/decompression. First, we see that the spread in attempt frequencies is much smaller in the silica glasses than in the LJ glasses, only about 4 orders of magnitude, although we should note that this range remains much larger than usually anticipated. Moreover, a weak but positive frequency dependence on the activation energy is seen here, which is in contrast with LJ glasses where the attempt frequency was reported to decrease with the activation energy. This might be due to the fact that thermally-activated events in silica glasses are rather localized in comparison with LJ glasses. In Fig. 9(a), there is also a slight shift towards lower frequencies in more rapidly quenched glasses, as reported for LJ glasses [44], while upon a cycle of compression/decompression (Fig. 9(b)), there is a clear decrease in the activation energies as reported above, but no effect on the range of attempt frequencies.

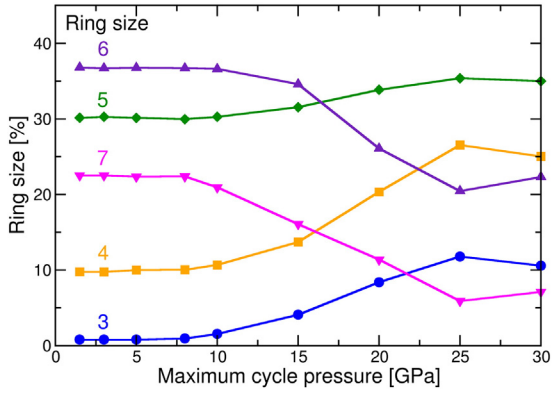

Fig. 7. Ring size distribution in glasses after decompression to zero pressure as a function of the maximum pressure reached during the compression cycle.

5. Conclusions

This work shows that, with the present interatomic potential, the SRO and MRO transitions are the signature of a single structural transition, which takes place gradually between about 8 and 25 GPa. Both the coordination number, ring size distribution and densification evolve together and all become irreversible during compression/decompression cycles at the same pressure, slightly below 8 GPa. This pressure is lower but close to the experimentally reported densification threshold, 10 GPa. Structurally, this transition corresponds to a progressive alteration of the tetrahedral structure of the glass. As the density increases, the Si atoms and their first neighbor O atoms are forced closer together, which increases the coordination of the Si atoms and their connectivity with other Si atoms through Si–O–Si bonds, which in turn reduces the size of the closed rings that connect the pair of bonds on the Si atoms. The fact that the SRO transition is irreversible contradicts experiments [15] and is related to our simulations to the presence after decompression of a large fraction of fivefold coordinated atoms. Such coordination

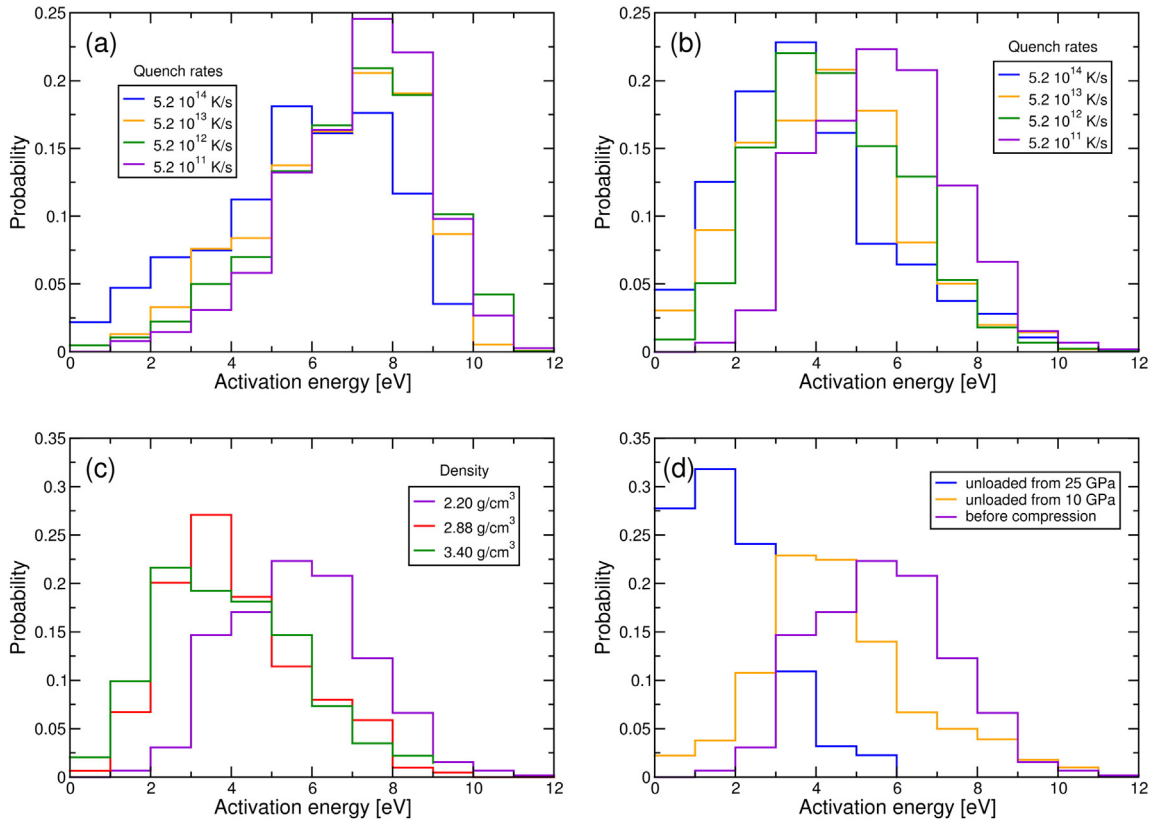

Fig. 8. Distributions of activation energies: (a) when only O atoms are involved, (b) when both Si and O atoms are involved, (c) in glasses quenched at different densities at the slowest quenched rate and when both Si and O atoms are involved, (d) in the initial glass and after a cycle of compression/decompression also when both Si and O atoms are involved.

defects have been reported experimentally and are seen in ab initio calculations [19], however to our knowledge, only one potential, which includes the polarizability of the O atoms, was reported to simulate a reversible SRO transition [23] (Huang and Kieffer [22] reported an irreversible change of MRO without change of SRO but they predicted an increase of the average ring size, which contradicts the experiments). Little detail was however given and it would be interesting to reproduce the present analysis with this polarizable potential to better understand the interplay between the MRO and SRO.

The second interesting observation from this work is that as-quenched glasses and glasses under compression have similar SRO and MRO when plotted as a function of density. The evolution of the latter during compressions is therefore not specific to the effect of plastic events on atomic environments, but rather results from steric effects, since similar variations are obtained with two very different routes to produce the glasses. Upon decompression on the other hand, there is a hysteresis, which means that the SRO and MRO are not just functions of the density but also depend on the history of the glass in decompression. However, this dependence remains limited since the hysteresis is small, in particular for the coordination number. Moreover, this history dependence disappears when the deformed glasses are brought back to their initial density, with both the MRO and SRO back to almost their initial values.

Interpreting these results in relation to the phenomenology of polyamorphism, it had already been observed that glasses with the same density could have different MROs and SROs. Here we show that, with the as-quenched glasses on the one side and the deformed glasses on the other, we can produce glasses with the same density, similar SRO and MRO, but significantly different pressures. The geometrical quantities, like coordination number and ring distributions, do not

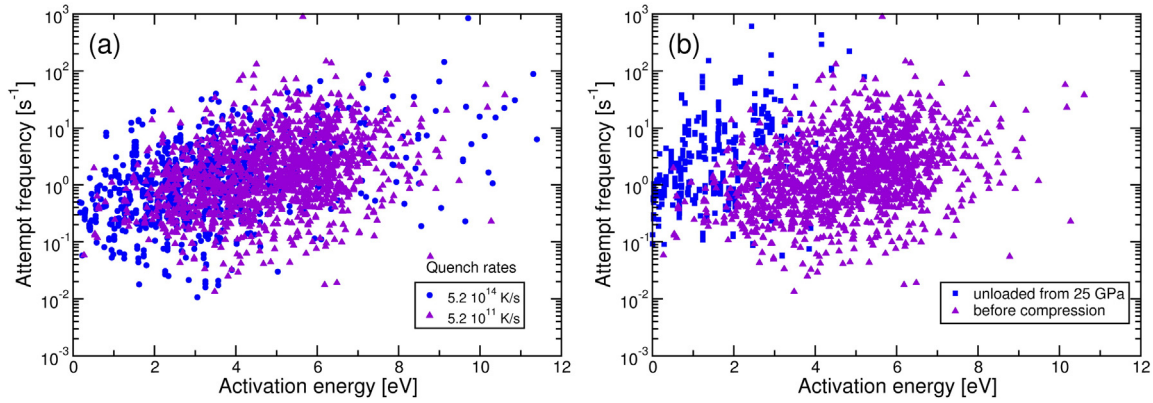

Fig. 9. Relation between the attempt frequency and activation energy of events involving both Si and O atoms, (a) in glasses quenched at different quench rates, (b) in the initial glass and after a cycle of compression/decompression.

clearly differentiate between these glasses. On the other hand, their local potential energy landscapes are significantly different, with the deformed glasses having the typical activation energy distribution of far-from-equilibrium systems, which contains a much higher density of low activation energies than as-quenched glasses.

Acknowledgments

The present work was funded by the Communautés de Recherche Académique (ARC) of the Région Rhône-Alpes, France. JLB and DR acknowledge funding from the Institut Universitaire de France.

References

[1] B. Mysen, P. Richet, Silicate Glasses and Melts, Elsevier B.V., The Netherlands, 2005.
[2] P. Bridgman, I. Simon, J. Appl. Phys. 24 (1953) 405.
[3] M. Grimsditch, Phys. Rev. 52 (1984) 2379.
[4] O. Tsiok, V. Brazhkin, A. Lyapin, L. Khvostantsev, Phys. Rev. Lett. 80 (1998) 999.
[5] C. Sonneville, T. Deschamps, C. Martinet, D. de Ligny, A. Mermet, B. Champagnon, J. Non-Cryst. Solids 382 (2013) 133.
[6] D. Vandembroucq, T. Deschamps, C. Coussa, A. Perriot, E. Barthel, B. Champagnon, C. Martinet, J. Phys. Condens. Matter 20 (2008) 485221.
[7] R. Hemley, H. Mao, P. Bell, B. Mysen, Phys. Rev. Lett. 57 (1986) 747.
[8] C. Sonneville, A. Mermet, B. Champagnon, C. Martinet, J. Margueritat, D. de Ligny, T. Deschamps, F. Balima, J. Chem. Phys. 137 (2012) 124505.
[9] S. King, Nature 213 (1967) 1112.
[10] C. Marians, L. Hobbs, J. Non-Cryst. Solids 106 (1988) 309.
[11] F. Galeener, J. Mikkelsen, Phys. Rev. B 23 (1981) 5527.
[12] F. Galeener, Phys. Rev. B 19 (1979) 4292.
[13] C. Meade, R. Hemley, H. Mao, Phys. Rev. Lett. 69 (1992) 1387.
[14] C. Benmore, E. Soignard, S. Amin, M. Guthrie, S. Shastri, P. Lee, J. Yarger, Phys. Rev. B 81 (2010) 054105.
[15] J. Lin, et al., Phys. Rev. B 75 (2007) 012201.
[16] T. Sato, N. Funamori, Phys. Rev. Lett. 101 (2008) 255502.
[17] V. Brazhkin, Phys. Rev. Lett. 102 (2009) 209603.
[18] N. Funamori, T. Sato, Phys. Rev. Lett. 102 (2009) 209604.
[19] M. Wu, Y. Liang, J. Jiang, J. Tse, Sci. Rep. 2 (2012) 398.
[20] Y. Inamura, Y. Katayama, W. Utsumi, K. Funakoshi, Phys. Rev. Lett. 93 (2004) 015501.
[21] D. Rodney, A. Tanguy, D. Vandembroucq, Model. Simul. Mater. Sci. Eng. 19 (2011) 083001.
[22] L. Huang, J. Kieffer, Phys. Rev. B 69 (2004) 224204.
[23] Y. Liang, C. Miranda, S. Scandolo, Phys. Rev. B 75 (2007) 024205.
[24] B. Mantisi, A. Tanguy, G. Kermouche, E. Barthel, Eur. Phys. J. B 85 (2012) 304.
[25] J. Tse, D. Klug, Y. Le Page, Phys. Rev. B 46 (1992) 5933.
[26] R. Della Valle, E. Venuti, Phys. Rev. B 54 (1996) 3809.
[27] D. Lacks, Phys. Rev. Lett. 80 (1998) 5385.
[28] K. Trachenko, M. Dove, Phys. Rev. B 67 (2003) 064107.
[29] P. Hung, N. Nhan, Scripta Mater. 63 (2010) 12.
[30] L. Huang, J. Kieffer, Phys. Rev. B 69 (2004) 224203.
[31] B. van Beest, G. Kramer, R. van Santen, Phys. Rev. Lett. 64 (1983) 1955.
[32] A. Carré, L. Berthier, J. Horbach, S. Ispas, W. Kob, J. Chem. Phys. 127 (2007) 114512.
[33] K. Vollmayr, W. Kob, K. Binder, Phys. Rev. B 54 (1996) 15808.
[34] J. Reinisch, A. Heuer, Phys. Rev. Lett. 95 (2005) 155502.
[35] H. Sheng, W. Luo, F. Alamgir, J. Bai, E. Ma, Nature 439 (2006) 419.
[36] Voro++. [link] URLhttp://math.lbl.gov/voro++s/.
[37] J. Rino, I. Ebbsjö, R. Kalia, A. Nakano, P. Vashishta, Phys. Rev. B 47 (1993) 3053.
[38] S. Le Roux, P. Jund, Comput. Mater. Sci. 49 (2010) 70.
[39] R. Malek, N. Mousseau, Phys. Rev. E. 62 (2000) 7723.
[40] E. Cancès, F. Legoll, M. Marinica, K. Minoukadeh, F. Willaime, J. Chem. Phys. 130 (2009) 114711.
[41] D. Rodney, C. Schuh, Phys. Rev. B 80 (2009) 184203.
[42] D. Rodney, C. Schuh, Phys. Rev. Lett. 102 (2009) 235503.
[43] D. Rodney, T. Schroder, Eur. Phys. J. E 34 (2011) 100.
[44] P. Koziatek, J.-L. Barrat, P. Derlet, D. Rodney, Phys. Rev. B 87 (2013) 224105.
[45] M.K.L. Library. [link], URLhttp://software.intel.com/en-us/intel-mkl.
[46] G. Walrafen, P. Krishnan, J. Chem. Phys. 74 (1981) 5328.